Front. Earth Sci. 2020, 14(4): 816–827
https://doi.org/10.1007/s11707-020-0820-6

RESEARCH ARTICLE

Characterizing the effects of climate change on short-term post-disturbance forest recovery in southern China from Landsat time-series observations (1988–2016)

Fangyan ZHU[1,2], Heng WANG[1,2], Mingshi LI (✉)[1,2], Jiaojiao DIAO[1,2], Wenjuan SHEN[1,2], Yali ZHANG[1,2], Hongji WU[1,2]

1 College of Forestry, Nanjing Forestry University, Nanjing 210037, China
2 Co-Innovation Center for Sustainable Forestry in Southern China, Nanjing Forestry University, Nanjing 210037, China

Abstract Climate change, a recognized critical environmental issue, plays an important role in regulating the structure and function of forest ecosystems by altering forest disturbance and recovery regimes. This research focused on exploring the statistical relationships between meteorological and topographic variables and the recovery characteristics following disturbance of plantation forests in southern China. We used long-term Landsat images and the vegetation change tracker algorithm to map forest disturbance and recovery events in the study area from 1988 to 2016. Stepwise multiple linear regression (MLR), random forest (RF) regression, and support vector machine (SVM) regression were used in conjunction with climate variables and topographic factors to model short-term forest recovery using the normalized difference vegetation index (*NDVI*). The results demonstrated that the regenerating forests were sensitive to the variation in temperature. The fitted results suggested that the relationship between the *NDVI* values of the forest areas and the post-disturbance climatic and topographic factors differed in regression algorithms. The RF regression yielded the best performance with an R^2 value of 0.7348 for the validation accuracy. This indicated that slope and temperature, especially high temperatures, had substantial effects on post-disturbance vegetation recovery in southern China. For other mid-subtropical monsoon regions with intense light and heat and abundant rainfall, the information will also contribute to appropriate decisions for forest managers on forest recovery measures. Additionally, it is essential to explore the relationships between forest recovery and climate change of different vegetation types or species for more accurate and targeted forest recovery strategies.

Received September 10, 2019; accepted February 14, 2020

E-mail: nfulms@njfu.edu.cn

Keywords climate change, forest disturbance, forest recovery, vegetation change tracker

1 Introduction

Climate change studies have enhanced our understanding of the climate system (Parmesan and Yohe, 2003). The temperature on the surface of the Earth between 1880 and 2012 has increased by 0.85°C, and according to the report by the Intergovernmental Panel on Climate Change, the years 2003 to 2012 were the warmest (IPCC, 2014). Greenhouse gas emissions are increasing due to the impact of human activities (Li et al., 2014). It has been suggested that forests are sensitive to climate change (Upgupta et al., 2015; Wang et al., 2016) and the disturbance of natural or human-induced events – such as clearcutting, thinning, and droughts (Chrysopolitou et al., 2013; Xin et al., 2013) – alters the ecological patterns of forests. Forest recovery from these disturbances equates to a strong carbon sink and plays a vital role in the global carbon cycle (Pan et al., 2011). Forest recovery influences the climate through biophysical mechanisms (Pan et al., 2011; O'Halloran et al., 2012). Theoretically, post-disturbance forest recovery is restricted by many on-site factors, including the type and magnitude of the disturbance, regeneration strategies, topography, and local climate (Meng et al., 2015; Roopsind et al., 2017).

To better understand the relationship between climate and post-disturbance forest recovery will benefit the sustainable management of the forests. It is a fundamental work to collect data on forest cover changes and remote sensing provides an efficient, viable, and reliable means to receive the up-to-date information. Huang et al. (2010) developed an algorithm called the vegetation change

tracker (VCT) for detecting forest change and mapping the changes in forest cover using Landsat time series stacks. The algorithm is based on the spectral-temporal characteristics of land cover and forest change processes. The mapping performance and good accuracy of the VCT have been documented in many regions, including Alabama, USA (Li et al., 2009), the Ning-zhen mountains, China (Li et al., 2016), and other locations where Landsat time-series stacks have been collected through the North American Forest Dynamics (NAFD) project (Goward et al., 2008; Huang et al., 2009). The VCT algorithm is a highly automatic and high-precision algorithm that enables the detection and tracking of forest change. Thus, the VCT substantially simplifies the task of obtaining information on forest disturbance and recovery in areas of frequent forest management practices, such as in the plantations of Southern China (Li et al., 2011; Shen et al., 2018; Shen et al., 2019).

Although empirical models have been used to simulate the status of post-disturbance forest recovery, relevant studies were primarily conducted in temperate continental climates, Mediterranean climates, and plateau climates (Meng et al., 2015; Liu, 2016; Pang et al., 2017). Some studies were performed on the impact of climate change on forest recovery. For example, Savage (1991) illustrated that adverse climatic conditions shortened the recovery time of pine forests. In a study of post-fire recovery of a pine-oak mixed forest in New York State, Meng et al. (2018) found that very high temperatures were highly correlated with the normalized difference vegetation index (*NDVI*). In contrast, it was concluded that higher temperatures and less precipitation might lead to a decline in carbon storage during the forest recovery process (Mccauley et al., 2019).

This research currently focuses on southern China, which has a mid-subtropical monsoon climate and plantation forests are dominant. The objective of this study is to investigate the trends of forest disturbance and the effects of climate change on forest recovery after disturbance in the plantation-dominated forests of southern China. The results are expected to provide insights for forest management in subtropical climates.

2 Materials and methods

2.1 Study site

The study area is located at the junction of Guangdong, Fujian, and Jiangxi provinces of China and includes the administrative cities of Ganzhou, Heyuan, Meizhou, and Longyan. The area is covered by the Landsat World Reference system-2 path/row 121/043 tile, with undulating topography of elevation ranges from 37 m to 1541 m. The area has a mid-subtropical monsoon climate, with an average annual precipitation of 1030 mm to 2000 mm and an average annual temperature of 19°C to 21°C. The rainy season ranges from March to September and about 50% of rainfall occurs between March and early July. The major forest types include the dominant subtropical evergreen broad-leaved forest, coniferous forest, and coniferous and broad-leaved mixed forest, and the tree main species are *Pinus massoniana*, *Cunninghamia lanceolata*, *Pinus elliottii Engelm, Eucalyptus, Pinus kwangtungensis, Castanopsis fissa, Acacia mangium, and Phyllostachys edulis.* The most common meteorological disturbances in the region are chilling injury of the plants, storms, flooding, and drought.

2.2 Data sets

Landsat time-series stacks consisting of approximately yearly Landsat Thematic Mapper (TM)/Enhanced Thematic Mapper (ETM+)/Operational Land Imager (OLI) images from 1988 to 2016 were assembled to enable the establishment of a historical record of forest disturbance and recovery in the plantations. The images were downloaded from the United States Geological Survey Earth Resources Observation and Science (USGS EROS) Center (available at USGS website). The following rules of the choice of images are to ensure the accuracy in the detection of forest changes: 1) the image acquisition dates had to fall in the growing season (mid-June to mid-September in the subtropical region), and 2) the images had to have minimal or no cloud contamination. No ETM+ images acquired after May 2003 were used, as there was a data gap caused by the scan line corrector (SLC) failure (Pringle et al., 2009). For images with relatively high cloud contamination, we obtained two or three of them in the same growing season with lower levels of cloud cover and different cloud locations to composite a new image with less cloud cover. A summary of the 27 Landsat scenes used in this study is provided in Table 1.

Climate data were obtained from the Ground Station database of the China Meteorological Administration, which provides annual data. We used annual precipitation, maximum and minimum temperatures, mean maximum and minimum temperatures, and mean temperature from 1988 to 2016 for the Shanghang, Wuhua, Meixian, Lianping, Xunwu, and Heyuan stations in the study area. We used co-kriging, a special case of ordinary kriging (Liu et al., 2006), to interpolate the climate variables in the study area. Geostatistical analyses and co-kriging interpolation were implemented in the GS + and ArcGIS 10.3 packages.

2.3 Data processing

2.3.1 Landsat data processing

The implementation of the VCT algorithm requires

Table 1 Landsat TM/ETM + /OLI scenes used in this analysis (WRS2 path/row = 121/043)

Image index	Acquisition date	Satellite	Sensor	Image quality
1	10/16/1988	Landsat 5	TM	High
2	07/15/1989	Landsat 5	TM	10% cloud coverage
3	10/22/1990	Landsat 5	TM	17% cloud coverage
4	09/23/1991	Landsat 5	TM	5% cloud coverage
5	10/09/1991	Landsat 5	TM	High
6	10/11/1992	Landsat 5	TM	16% cloud coverage
7	10/01/1994	Landsat 5	TM	High
8	09/18/1995	Landsat 5	TM	5% cloud coverage
9	10/20/1995	Landsat 5	TM	14% cloud coverage
10	08/20/1999	Landsat 7	ETM+	1% cloud coverage
11	10/17/2000	Landsat 5	TM	14% cloud coverage
12	05/13/2001	Landsat 5	TM	High
13	08/28/2002	Landsat 7	ETM+	24% cloud coverage
14	10/07/2002	Landsat 5	TM	41% cloud coverage
15	07/06/2003	Landsat 5	TM	27% cloud coverage
16	07/22/2003	Landsat 5	TM	2% cloud coverage
17	09/26/2004	Landsat 5	TM	1% cloud coverage
18	08/12/2005	Landsat 5	TM	1% cloud coverage
19	10/05/2007	Landsat 5	TM	High
20	09/21/2008	Landsat 5	TM	6% cloud coverage
21	10/26/2009	Landsat 5	TM	High
22	10/29/2010	Landsat 5	TM	High
23	08/10/2010	Landsat 5	TM	23% cloud coverage
24	07/28/2011	Landsat 5	TM	5% cloud coverage
25	09/19/2013	Landsat 8	OLI	4% cloud coverage
26	10/08/2014	Landsat 8	OLI	3% cloud coverage
27	09/27/2016	Landsat 8	OLI	High

Landsat surface reflectance images in standard format and the band combinations of Blue, Green, Red, NIR (Near Infrared), SWIR1 (Short Wave Infrared 1), SWIR2 (Short Wave Infrared 2), and the thermal bands. The Landsat TM/ETM+ images were orthorectified with subpixel accuracy. The data were radiometrically and atmospherically corrected to surface reflectance by applying the Landsat Ecosystem Disturbance Adaptive Processing System (LEDAPS) algorithm, which is a high-level automatic pre-processing algorithm for TM/ETM+ images (Masek et al., 2006). The Landsat 8 OLI image products include surface reflectance products generated by the Landsat Surface Reflectance Code (LaSRC) from the USGS EROS Data Center. This method uses three sources of information: 1) the coastal aerosol band (to perform aerosol inversion tests), 2) auxiliary climate data from MODIS, and 3) a radiative transfer model (Landsat Surface Reflectance Level-2 Science Data Products, available at USGS website (Vermote et al., 2016)).

2.3.2 Mapping and validation of forest disturbance and recovery

The Landsat time series stacks were analyzed with the VCT algorithm to obtain the disturbance parameters (Huang et al., 2010). For example, the algorithm provides several parameters, including disturbance maps, year of disturbance, and disturbance magnitude; these parameters are based on the spectral-temporal characteristics of land cover and forest change. The VCT algorithm consists of two main steps, including individual image analysis and time series analysis. The VCT model tracks forest changes using an integrated forest *z*-score (*IFZ*). The calculation formula of the *IFZ* is as follows:

$$FZ_i = \frac{b_i - \overline{b_i}}{SD_i}, \quad (1)$$

where $\overline{b_i}$ and SD_i represent the mean and standard

deviation of the spectral value of the forest pixel of each band, respectively, and b_i represents any pixel in the image. For multi-spectral images, the *IFZ* value is defined by integrating *FZi* over the spectral bands as follows:

$$IFZ = \sqrt{\frac{1}{NB}\sum_{i=1}^{NB}(FZ_i)^2}, \quad (2)$$

where *NB* represents the number of bands used. For the Landsat TM/ETM+ images, bands 3, 5, and 7 were used to calculate the *IFZ* values, and for the Landsat OLI images, bands 4, 6, and 7 were used. The *IFZ* is an inverse measure of the likelihood of each pixel being a forest pixel. If the *IFZ* value is low (0.3 for dense forests and 0.2 for sparse forests) and relatively stable throughout the monitoring period, we determined that the pixel represented persisting forest. A sharp increase in the *IFZ* value during a specific year indicates the occurrence of a disturbance in that year. Forest recovery was defined as the gradual decrease in the *IFZ* from high values. To avoid false positives, VCT uses the consecutive high integrated forest *z*-score values which were recorded following an integrated forest *z*-score hike to determine whether the increase was caused by a noisy observation or a disturbance (Huang et al., 2010). In this study, we focused on the disturbance maps because they allowed us to determine where and when disturbances had occurred. A detailed description of the disturbance maps is listed in Table 2. We adopted the validation method proposed by Li et al. (2016) that uses three randomly identified 3 km × 3 km plots. The validation process is shown in Fig. 1. The spatial agreement index was calculated by comparing the VCT detection results with the visual interpretations of the corresponding Google Earth images or Landsat image pairs at an earlier date in the period if Google images were not available. The spatial agreement index is defined as follows:

$$SAI = \frac{Scd}{Sg}. \quad (3)$$

In this method, the area of the disturbance region identified by the VCT is defined as *Sv*. The area of the disturbance region determined by the visual interpretations of the Google Earth images is *Sg*. *Scd* is the overlap area of the two detected regions.

2.3.3 Forest recovery analysis based on *NDVI* time series

We focused on the disturbances that occurred between 1989 and 2010 due to the time limitation of the available Landsat observations. Previous studies have indicated the *NDVI* value was efficient in characterizing vegetation recovery status (Díaz-Delgado et al., 2002; van Leeuwen et al., 2010). It has been hypothesized that an increase in the *NDVI* value following disturbance results in an increase in the cover of trees, shrubs, and herbaceous vegetation (Meng et al., 2015). However, the disadvantage of using the *NDVI* to estimate vegetation conditions is the saturation of the *NDVI* in dense vegetation canopies or areas with a high leaf area index (Carlson et al., 1990). This study focused on the early stages of vegetation recovery to minimize the saturation effect, i.e., we used the *NDVI* values from the first 5 years (excluding the first-year post-disturbance) to represent the recovery status of the disturbed forest patches and investigate the effects of short-term forest recovery. Specifically, we used the recovery trend index (*RTI*) in the initial stages of rapid regrowth. The index is a measure of the recovery trend that uses the slope of a line fitted by the Theil-Sen estimator (João et al., 2018). Here, we used the post-disturbance *NDVI* trend. Since the Theil-Sen estimator is a rank-based test, it is insensitive to a non-normal distribution and missing values (Theil, 1992). We used the *mblm* package in *R*. 3.4.2. for statistical analyses (Wang, 2018).

2.3.4 Modeling forest recovery following disturbance

Based on previous studies (Meng et al., 2015; Zhao et al., 2016; Luo et al., 2017), different environmental variables were used to assess the effects of disturbance (post-disturbance *NDVI* values and the disturbance magnitude), topography (elevation, slope, and aspect), and climatic factors on forest recovery (see Table S1 for more details on the variables). The disturbance magnitude in this study was calculated using the *IFZ*. We chose 70–150 points in

Table 2 Definition and aggregation of forest disturbance maps developed from VCT

Value	Class description in VCT model	Aggregated class
0	Background area	Abandoned
1	Persisting nonforest	Nonforest
2	Persisting forest	Forest
4	Persisting water	Nonforest
5	Previously disturbed but spectrally restored to forest this year	Forest
6	Disturbed in this year	Nonforest
7	Post-disturbance nonforest	Nonforest

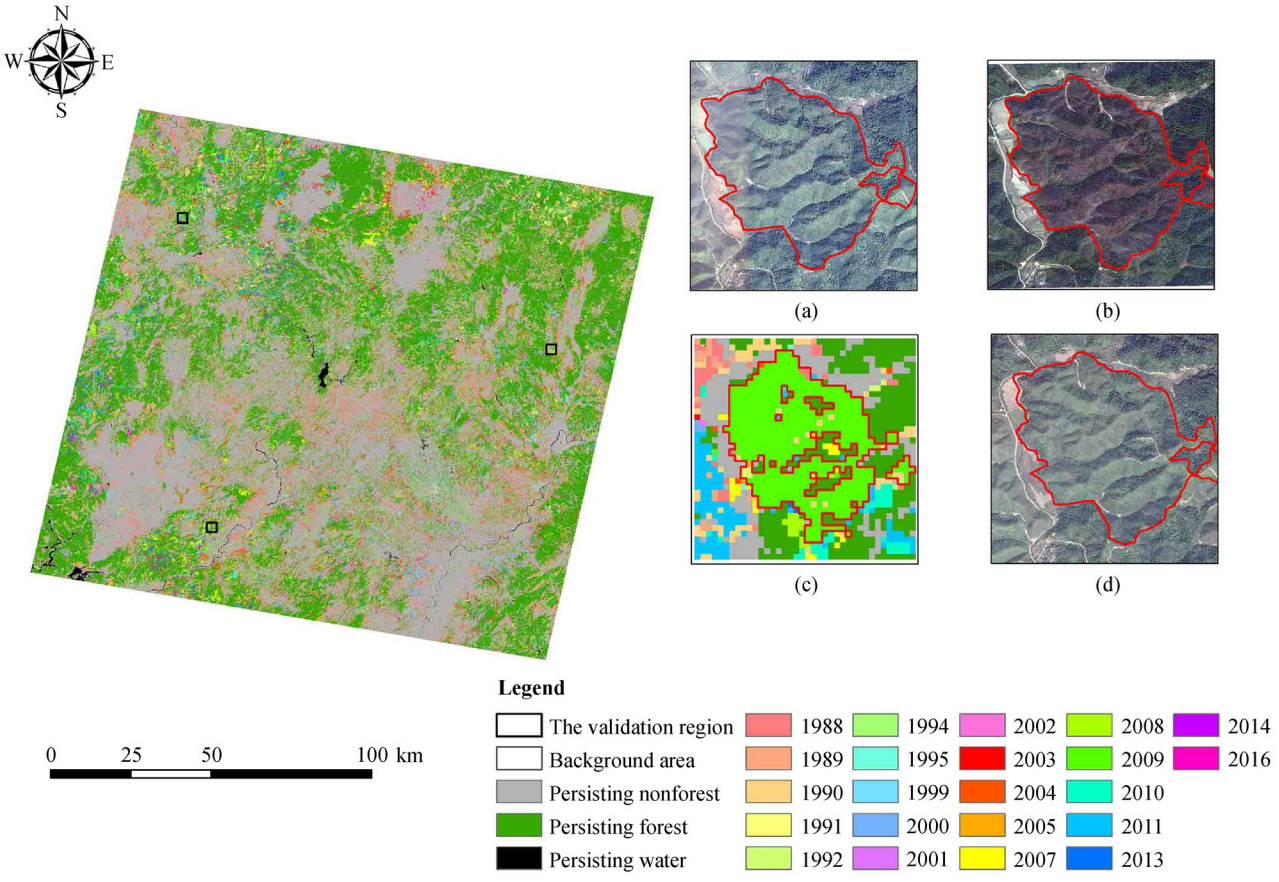

Fig. 1 Forest disturbance patterns mapped by the VCT algorithm, 1988–2016. The three black squares with a side length of 3 km are the validation plots that were randomly identified on the disturbance map. The four images on the right show the validation process of the eastern plot: (a) Google Earth image in 2008; (b) Google Earth image in 2009; (c) year of disturbance (showing the disturbance that occurred in 2009); (d) Google Earth image in 2016. Spatial agreement = the area of agreement area between (b) and (c) divided by the area of (b).

disturbed patches and extracted the pixel values (see Table S1); 70% of the data were used as training data, and the rest was used to test the reliability of the models. The relationships between the climate variables, topography, disturbance, and forest recovery were assessed using three types of regression models, i.e., stepwise multiple linear regression (MLR), random forest (RF), and support vector machine (SVM) models. The results of the best model were used for the analysis.

The stepwise MLR model was used to identify and quantify the relationships between the *NDVI* for the fifth year and the predictor variables. The stepping criteria for the addition and removal of the variables were based on the significance level (F-value equals to 0.05). Prior to statistical modeling, min–max normalization was carried out for root morphological parameters and tissue compositions to prevent attributes with large numeric ranges from dominating those with small numeric ranges. Min–max normalization involved subtracting the minimum value of an attribute from each value of the attribute and then dividing the difference by the range of the attribute. The normalized values ranged between 0 and 1. The advantage of this normalization is that it preserves the relationships of the data values and does not introduce potential bias into the data. Stepwise multiple linear regression model constructs a multivariate model based on a few deliberately selected explanatory variables. The best model was selected on the basis of the highest multiple correlation coefficient (R^2) (Zhan et al., 2013). Stepwise multiple linear regression model was evaluated using the *mblm* package in *R*.

RF is a non-parametric algorithm with the following advantages over MLR models: 1) the variable importance can be determined; 2) it is robust to data reduction; 3) there is no risk of overfitting; 4) it generates unbiased accuracy estimates and decision trees; 5) it has high accuracy and low sensitivity to the adjustment of parameters (Breiman, 2001). The weaknesses of the RF modeling are that the decision rules are unknown (black box) and the implementation is computationally expensive. We used the RF model in the R-package and identified the important predictors to determine the relationships between the

predictors and *NDVI* for the fifth year. There were 500 trees (ntree) for modeling, and each tree was created from four-fifths of a random sampling of the training data. For the parameter mtry, we used the default value of the square root of the total number of predictor variables. The node size was set to the default value of 1.

SVM regression model is a more advanced statistical method compared to traditional linear and nonlinear regressions. SVM regression model is a supervised and non-parametric machine-learning algorithm for classification and regression analyses. This method offers many unique advantages in dealing with small-sized samples, nonlinear and high dimensional pattern recognition, and is highly correlated with predictor variables.

It is worth noting that the predictors used in the RF and SVM regression models were selected using the importance function in the RF model. The importance of the predictor was assessed using the mean square error (MSE) (percent IncMSE) and the node purity (IncNode Purity). The less important predictors were removed from the model, and a small subset of predictors was selected to create the optimum model.

3 Results

The spatiotemporal pattern of the forest disturbances presented when and where, and the number of forest disturbance events had occurred in the past 29 years (Fig. 1). The forest disturbance rate ranged from 0.47% (1995) to 3.15% (2009) and fluctuated between 0.7% and 2.0%. It was assumed that this range represented the normal level of forest disturbance in the study area (Fig. 2). There was an increase in the disturbance rate in 2008 and 2009 – the images indicated large-scale forest disturbance – which was attributed to extreme winter weather that affected the south-central region of China from 10 January to 8 February 2009 (Zhou et al., 2011) (Fig. 2). Not any particular trend did the forest recovery rates have but only a fluctuation between 0.63% (2002) and 3.74% (1995) (Fig. 2). Most of the recovery rates were between 0.8% and 2.0%, but there were two peaks (1995 and 2013), which corresponded to the disturbances that had occurred several years previously. The results of the spatial agreement obtained from the three plots are listed in Table 3. The values ranged from 59.89% to 92.35%, with most measurements being between 70.0% and 86.0%.

The slope based on the Theil-Sen estimator represents the *RTI*, is showing the trend of forest recovery. The *NDVI* values tended to increase with increasing *RTI* values. Forest recovery occurred faster after disturbances in 2009, 2010, and 2011 but slower after disturbances in 1990 (Fig. 3). We found that *NDVI*_1 (which was used as a proxy for the condition of the post-disturbance vegetation), extremely high temperatures, and the slope were the most important variables; high temperature was the most reliable

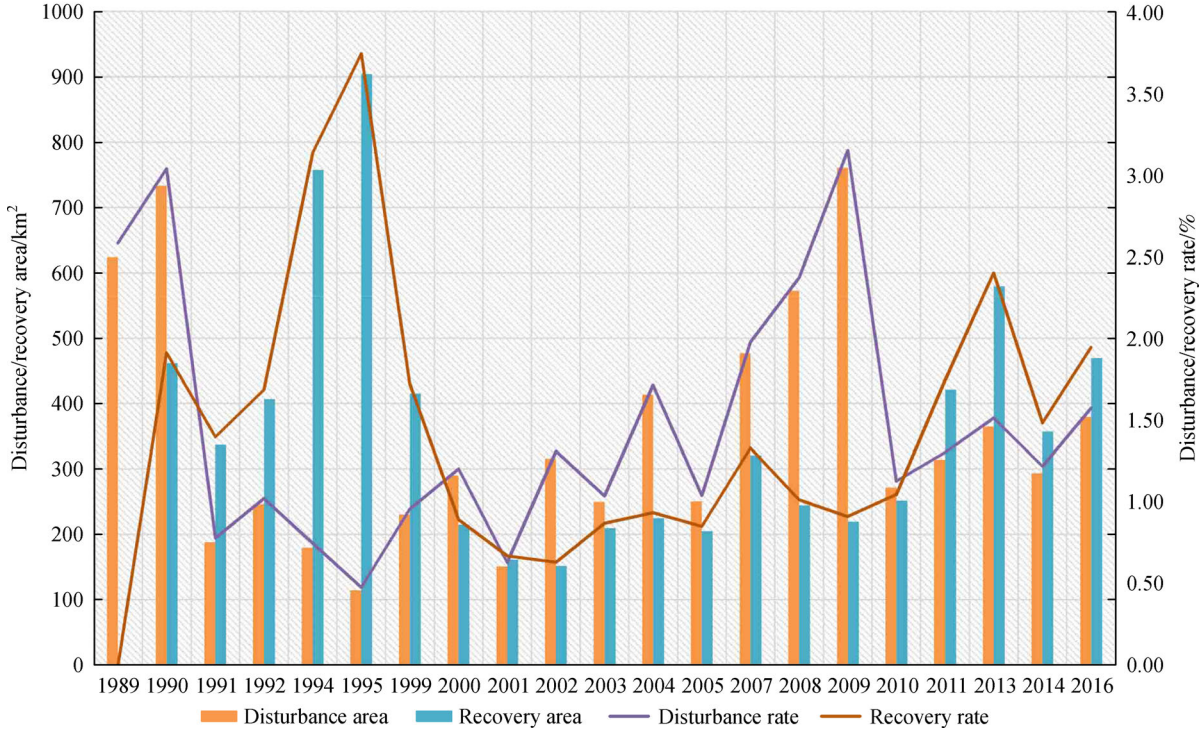

Fig. 2 Changes in the forest disturbance/recovery area and rates obtained from the VCT algorithm.

Table 3 Spatial agreement measurements of the 9 km^2 validation plots

Eastern plot		Middle plot		Western plot	
Disturbance year	Agreement measure/%	Disturbance year	Agreement measure/%	Disturbance year	Agreement measure/%
1989	74.54	1989	92.35	1989	78.15
1990	80.31	1990	91.50	1990	65.84
1991	59.89	1991	80.82	1991	69.31
1992	61.07	1992	71.10	1992	61.01
1995	84.03	1995	70.00	1995	72.54
2000	60.03	2000	60.48	2000	61.44
2001	67.20	2001	75.93	2001	77.89
2004	89.53	2004	60.57	2004	89.63
2005	81.27	2005	86.51	2005	72.32
2006	66.16	2006	74.24	2006	74.92
2007	86.83	2007	79.42	2007	70.08
2008	70.24	2008	73.91	2008	72.25
2009	66.82	2009	70.37	2009	62.31
2010	72.82	2010	73.40	2010	71.30
2011	76.61	2011	73.93	2011	71.65
2013	71.52	2012	78.34	2012	70.81
2014	69.36	2014	72.33	2014	80.12
2016	73.86	2016	74.25	2016	72.33

predictor (Fig. S1). Based on the analysis, we chose 25 variables to model post-disturbance forest recovery.

In this study, the fitting and verification accuracies were used to evaluate the model results. The three models' modeling contribution was evaluated by calculating R^2, Mean Relative Error (*MRE*), the Root Mean Square Error (*RMSE*), and comparisons between maximum, minimum, mean and observed values.

The RF model had the highest accuracy; the R^2 value was 0.9448 for the fitting accuracy and 0.7348 for the validation accuracy. Although the SVM regression model performed better than the RF model regarding fitting accuracy, overfitting of the data occurred (Tables 4 and 5).

4 Discussion

4.1 Forest disturbance and recovery characteristics

Figure 2 shows an anomaly of the forest disturbance rate in the study site in 2008 and 2009, and this peak was likely related to an exceptionally cold period with freezing rain and snow in 2008 (Zhou et al., 2011). The extreme cold inhibited the growth of forests and produced a significant amount of combustible materials (due to dead vegetation), which increased the risk of forest fire (Dale et al., 2001). Current forest disturbance monitoring in Jiangxi Province is based on a time-series trajectory of a remote sensing index. It has yielded results that are consistent with the data from 2001 to 2011 describing a known burned forest area in Jiangxi Province (Wu, 2014). The 1990 and 2009 Landsat images were acquired respectively on 22 and 26 October, i.e., during the late autumn or early winter for this mid-latitude region. The deciduous forest was likely in a leaf-off status during this time, which could have caused the VCT algorithm to flag these sites erroneously as areas of change. The disturbance area for the first year of the Landsat time series (1988) was extensive. At the beginning period of the study, there was no available spectral contrast from which to derive information on change; therefore, we used no disturbance data or forest recovery data from the first year of the image stack.

The majority of the study area is located in northern Guangdong, an under-developed mountainous area. Improper forest management is an important factor leading to the decline of forest quality (Sun et al., 2017), which in this area has resulted in substantial destruction of forest resources in the early 1980s (Xu, 1999). A 'greening' policy was put forward in Guangdong Province in 1985 and significantly reduced deforestation in this area. The disturbance rate during our research period did not exceed 3.15%. The priority for forest development in northern Guangdong Province since 2001 has been forestry and non-commercial forest construction (Liu et al., 2004). Many fast-growing and high-yield plantation forests have been created, changing the balance between the distur-

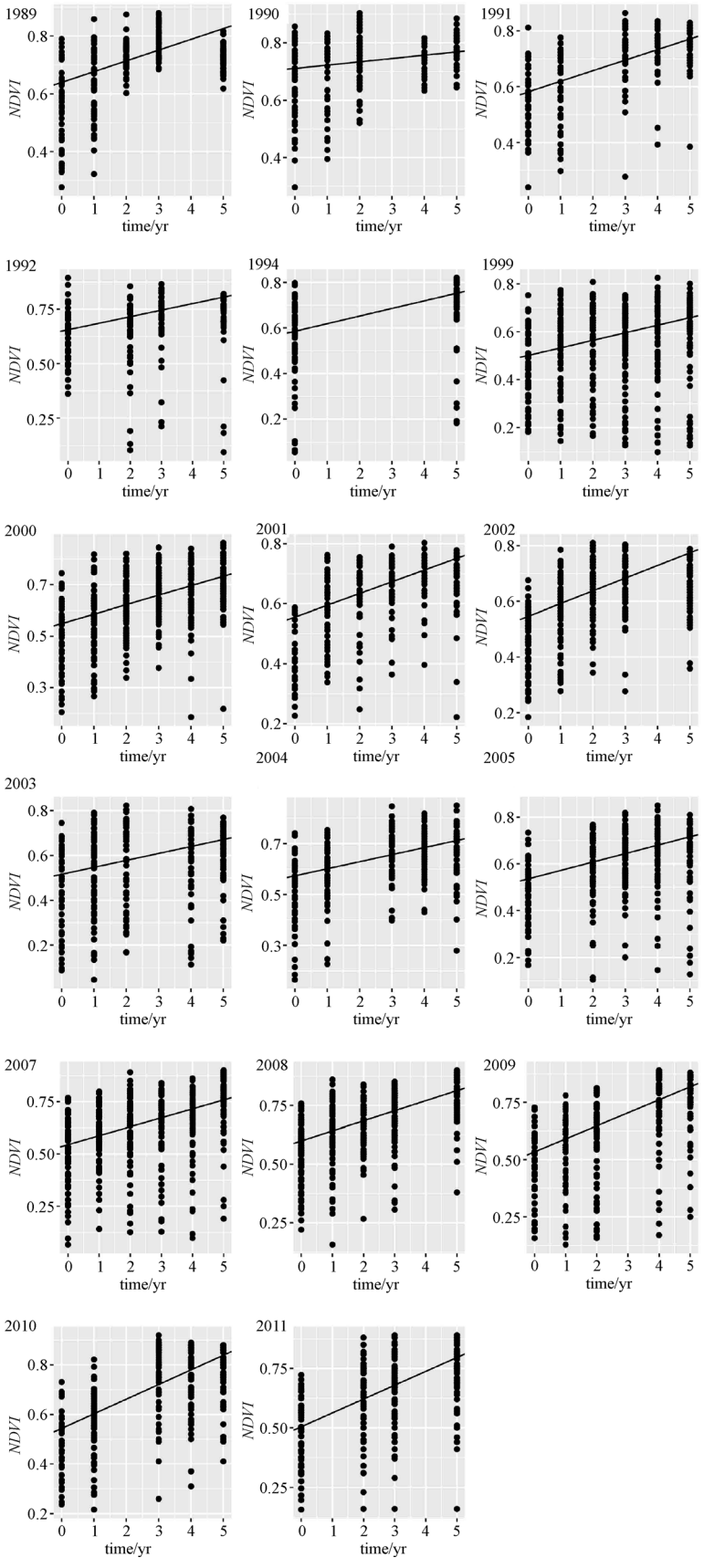

Fig. 3 Forest recovery trend based on the Theil-Sen estimation.

Table 4 Fitting accuracy

	R^2	*MRE*	*RMSE*	Maximum	Minimum	Mean
Stepwise LM	0.5475	0.0979	0.0028	0.9020	0.3348	0.6924
Random forest (RF)	0.9464	0.0345	0.0004	0.8430	0.1736	0.6920
SVM	0.9784	0.0196	0.0001	0.8719	0.1577	0.6911
Observed *NDVI*				0.883	0.1413	0.6924

Table 5 Validation accuracy

	R^2	*MRE*	*RMSE*	Maximum	Minimum	Mean
Stepwise LM	0.5814	0.1616	0.0044	0.8578	0.3798	0.6773
Random forest (RF)	0.7667	0.0714	0.0017	0.8170	0.2124	0.6783
SVM	0.6870	0.0803	0.0021	0.8200	0.2425	0.6758
Observed *NDVI*				0.8265	0.1615	0.6762

bance area and the recovery area between 2001 and 2016. Harvesting and low-intensity human-induced fires have long been the major causes of disturbance in the study area, according to the China Forestry Yearbook (National Forestry and Grassland Administration, 2018). The fast-growing and the high-yield plantation forests have short rotation cycles and have to be harvested regularly to allow regeneration. Prescribed burning has been commonly used in southern China for preparing the ground for seeding or planting after harvesting, particularly for Chinese fir (Sun et al., 2011).

There was a substantial increase in the forest recovery area after 1989 as a result of the biogeographic conditions in the study area. The mid-subtropical monsoon climate and abundant solar illumination and precipitation are conducive to vegetation growth and recovery in this particular region. The major tree species that were chosen for plantation establishment are fast-growing and have short rotation cycles. Professional forest management measures have ensured rapid forest recovery within several years of a disturbance.

Forest recovery that refers to the reestablishment of key forest biophysical variables following a disturbance event is a process rather than a state (Frolking et al., 2015). The recovery rate differs due to the magnitude and type of disturbance, the biogeographic conditions, and the climate (Bolton et al., 2013). Post-disturbance forest recovery occurs via multiple pathways, including no recovery (land-use change), artificial recovery, or natural recovery. Our results showed a slight increase in forest coverage, and the statistical analysis indicated that only about 1% of the disturbed forests in the study area showed no signs of recovery; nearly all remaining disturbed pixels changed to recovery pixels within 6 years. The disturbance and subsequent recovery events are key processes that shape the type and the age structure of forests and represent critical factors in the sustainable forest management of plantations in southern China.

4.2 Forest recovery response to climate

The modeling result indicated that climatic conditions in the first few post-disturbance years were the most important factors contributing to forest recovery. The relative importance of the predictor variables showed that high temperature was the most significant predictor of forest recovery (Fig. S1). Investigations of other forest areas have also revealed that high temperatures or drought stress affected vegetation growth (Sun et al., 2007; Mildrexler et al., 2016). In our study, high temperatures were correlated with the occurrence of fires, whose impact on forests would have been immediate. Precipitation did not explain the changes in the *NDVI* in this study because the prevailing climatic conditions of southern China are excellent for forest recovery. Thus, rainfall and sunshine were not the limiting factors for forest recovery in this particular region. Additionally, elevation was also not an influential factor in forest recovery, but the slope had a significant impact on forest recovery (Fig. S1). The reason may be that the slope affects forest soil fertility, sunlight and soil moisture, thus affecting tree growth and forest stand recovery, especially in steep locations. However, the temperature may be a critical factor for forest growth when enough moisture is available (Minore and Laacke, 1992), and temperature was an important factor in this study (Fig. S1). A comparison of the predictive performance of the three models indicated that the nonlinear model showed the best fit, presumably because the process of post-disturbance recovery is complex, and many of the site parameters have nonlinear interactions. Climatic effects are not temporary and interact with other processes since many climatic factors are linked with human activities. Topo-

graphy and the magnitude of disturbances were not powerful predictors in the regression model; the reason may be that the primary disturbance type (e.g., logging) in this area is anthropogenic. Topography might not have had a large impact on human management activities in this particular region.

Our results indicated that the following ideas should be considered in future studies: 1) The Landsat images and the vegetation index-based analysis made it difficult to distinguish the vegetation types and species. Different types of vegetation, and even different species of the same genus, respond differently to climate change (Meng et al., 2015; Zhen et al., 2011). Additional research is, therefore, required to explore the relationship between the recovery of different vegetation types or species and climate change using high-resolution remotely sensed data and forest management data. 2) The VCT products only identify the time and location that the disturbance or recovery events have occurred, but provide no information on the disturbance type. Climate is more closely related to natural disturbances (such as hurricanes or drought) than human activity. Subsequent investigations should focus on field-work to distinguish different disturbance types. In previous studies, it was demonstrated that the use of field data and the SVM algorithm was well suited for the detection of, and differentiation between, disturbances (Huang et al., 2002; Zhao et al., 2015). 3) Focused on the correlation between climate change and post-disturbance forest recovery in this research, we did not quantify the impact of climate change on forest recovery in the study area, and that is the direction we will focus on in the future.

5 Conclusions

This paper reported on the potential impacts of climate change on post-disturbance forest recovery. Climatic factors, particularly very high temperatures and slope were highly correlated with post-disturbance forest recovery in southern China. The results showed that the VCT algorithm provided insights into forest disturbances and recovery histories that are informative for interdisciplinary scientific applications. The findings also provided a solid basis for the strategic development of sustainable forest management plans in response to climate change, as well as a method for determining the carbon sequestration capacity of forest plantations using long-term data.

Acknowledgements We express our gratitude to the USGS EROS Center for providing the standardized Landsat images to support the analysis. This work was jointly supported by the National Natural Science Foundation of China (Grant Nos. 31971577 and 31670552), the Biodiversity Investigation, Observation and Assessment Program sponsored by the Ministry of Ecology and Environment of China (2019-2023), the China Postdoctoral Science Foundation (No. 2019M651842), and the Priority Academic Program Development of Jiangsu Higher Education Institutions (PAPD).

Eletronic Supplementary material is available in the online version of this article at https://doi.org/10.1007/s11707-020-0820-6 and is accessible for authorized users.

References

Bolton D K, Coops N C, Wulder M A (2013). Measuring forest structure along productivity gradients in the Canadian boreal with small-footprint Lidar. Environ Monit Assess, 185(8): 6617–6634

Breiman L (2001). Random forests. Mach Learn, 45(1): 5–32

Carlson T, Perry E, Schmugge T (1990). Remote estimation of soil moisture availability and fractional vegetation cover for agricultural fields. Agric Meteorol, 52(1–2): 45–69

Chrysopolitou V, Apostolakis A, Avtzis D, Avtzis N, Diamandis S, Kemitzoglou D, Papadimos D, Perlerou C, Tsiaoussi V, Dafis S (2013). Studies on forest health and vegetation changes in Greece under the effects of climate changes. Biodivers Conserv, 22(5): 1133–1150

Dale V, Joyce L, Mcnulty S, Neilson R P, Ayres M P, Flannigan M D, Hanson P J, Irland L C, Lugo A, Peterson C J, Simberloff D, Swanson F J, Stocks B J, Michael Wotton B (2001). Climate change and forest disturbances climate change can affect forests by altering the frequency, intensity, duration, and timing of fire, drought, introduced species, insect and pathogen outbreaks, hurricanes, windstorms, ice storms, or landslides. Bioscience, 51(9): 723–734

Díaz-Delgado R, Lloret F, Pons X, Terradas J (2002). Satellite evidence of decreasing resilience in Mediterranean plant communities after recurrent wildfires. Ecology, 83(8): 2293–2303

Frolking S, Palace M, Clark D, Chambers J, Shugart H, Hurtt G (2015). Forest disturbance and recovery: a general review in the context of spaceborne remote sensing of impacts on aboveground biomass and canopy structure. J Geophys Res Biogeosci, 114 (G2)

Goward S, Masek J, Cohen W, Moisen G, Collatz G J, Healey S, Houghton R A, Huang C, Kennedy R, Law B, Powell S, Turner D, Wulder M A (2008). Forest disturbance and North American carbon flux. Eos (Wash DC), 89(11): 105–116

Huang C, Davis L, Townshend J (2002). An assessment of support vector machines for land cover classification. Int J Remote Sens, 23 (4): 725–749

Huang C, Goward S, Masek J, Gao F, Vermote E F, Thomas N, Schleeweis K, Kennedy R E, Zhu Z, Eidenshink J C, Townshend J R G (2009). Development of time series stacks of Landsat images for reconstructing forest disturbance history. Int J Digit Earth, 2(3): 195–218

Huang C, Goward S, Masek J, Thomas N, Zhu Z, Vogelmann J (2010). An automated approach for reconstructing recent forest disturbance history using dense Landsat time series stacks. Remote Sens Environ, 114(1): 183–198

IPCC (2014). Intergovernmental Panel on Climate Change. Geneva: Fifth Assessment Report

João T, João G, Bruno M, João H (2018). Indicator-based assessment of post-fire recovery dynamics using satellite *NDVI* time-series. Ecol Indic, 89: 199–212

Li M, Huang C, Shen W, Ren X, Lv Y, Wang J, Zhu Z (2016). Characterizing long-term forest disturbance history and its drivers in

the Ning-Zhen Mountains, Jiangsu Province of eastern China using yearly Landsat observations (1987–2011). J For Res, 27(6): 1329–1341

Li M, Huang C, Zhu Z, Shi H, Lu H, Peng S (2009). Assessing rates of forest change and fragmentation in Alabama, USA, using the vegetation change tracker model. For Ecol Manage, 257(6): 1480–1488

Li M, Zhu Z, Vogelmann J, Xu D, Wen W, Liu A (2011). Characterizing fragmentation of the collective forests in southern China from multitemporal Landsat imagery: a case study from Kecheng district of Zhejiang Province. Appl Geogr, 31(3): 1026–1035

Li W, Wang Q, Shen L (2014). Impact of climate change on forest ecosystems and countermeasures of sustainable forest development. Forest Inventory and Planning, 1: 94–97

Liu X, Wu J, Xu J (2006). Characterizing the risk assessment of heavy metals and sampling uncertainty analysis in paddy field by geostatistics and GIS. Environ Pollut, 141(2): 257–264

Liu Y, Xu Z, Wen S, Zhang X (2004). Study on forest regional and industrial features and its strategic development in Guangdong Province. J South Chin Agric Univ, 2004(04): 50–57

Liu Z (2016). Effects of climate and fire on short-term vegetation recovery in the boreal larch forests of Northeastern China. Sci Rep, 6 (1): 819–822

Luo D, Huang J G, Jiang X, Ma Q, Liang H, Guo X, Zhang S (2017). Effect of climate and competition on radial growth of Pinus massoniana and Schima superba in China's subtropical monsoon mixed forest. Dendrochronologia, 46: 24–34

Masek J, Vermote E, Saleous N, Wolfe R, Hall F G, Huemmrich K F, Gao F, Kutler J, Lim T K (2006). A Landsat surface reflectance dataset for North America, 1990–2000. IEEE Geosci Remote Sens Lett, 3(1): 68–72

Mccauley L, Robles M, Woolley T, Marchall R, Kretchun A, Gori D (2019) Large-scale forest restoration stabilizes carbon under climate change in Southwest United States. Ecological Applications, 29(8): 1–14

Meng R, Dennison P, Huang C, Moritz M A, D'Antonio C (2015). Effects of fire severity and post-fire climate on short-term vegetation recovery of mixed-conifer and red fir forests in the Sierra Nevada Mountains of California. Remote Sens Environ, 171: 311–325

Meng R, Wu J, Zhao F, Cook B D, Hanavan R P, Serbin S P (2018). Measuring short-term post-fire forest recovery across a burn severity gradient in a mixed pine-oak forest using multi-sensor remote sensing techniques. Remote Sens Environ, 210: 282–296

Mildrexler D, Yang Z, Cohen W B, Bell D M (2016). A forest vulnerability index based on drought and high temperatures. Remote Sens Environ, 173: 314–325

Minore D, Laacke R J (1992). Natural Regeneration. Corvallis: Oregon State University Press,258–283

National Forestry and Grassland Administration (2018). China Forestry Yearbook. Beijing: China Forestry Publishing House

O'Halloran T, Law B, Goulden M, Wang Z, Barr J G, Schaaf C, Brown M, Fuentes J D, Göckede M, Black A, Engel V (2012). Radiative forcing of natural forest disturbances. Glob Change Biol, 18(2): 555–565

Pan Y, Birdsey R A, Fang J, Houghton R, Kauppi P E, Kurz W A, Phillips O L, Shvidenko A, Lewis S L, Canadell J G, Ciais P, Jackson R B, Pacala S W, McGuire A D, Piao S, Rautiainen A, Sitch S, Hayes D (2011). A large and persistent carbon sink in the world's forests. Science, 333(6045): 988–993

Pang G, Wang X, Yang M (2017). Using the *NDVI* to identify variations in, and responses of, vegetation to climate change on the Tibetan Plateau from 1982 to 2012. Quat Int, 444: 87–96

Parmesan C, Yohe G (2003). A globally coherent fingerprint of climate change impacts across natural systems. Nature, 421(6918): 37–42

Pringle M, Schmidt M, Muir J (2009). Geostatistical interpolation of SLC-off Landsat ETM + images. ISPRS J Photogramm Remote Sens, 64(6): 654–664

Roopsind A, Wortel V, Hanoeman W, Putz F (2017). Quantifying uncertainty about forest recovery 32-years after selective logging in Suriname. For Ecol Manage, 391: 246–255

Savage M (1991). Structural dynamics of a southwestern pine forest under chronic human influence. Ann Assoc Am Geogr, 81(2): 271–289

Shen W, Li M, Huang C, Tao X, Wei A (2018). Annual forest aboveground biomass changes mapped using ICESat/GLAS measurements, historical inventory data, and time-series optical and radar imagery for Guangdong province, China. Agric Meteorol, 259: 23–38

Shen W, Li M, Huang C, He T, Tao X, Wei A (2019). Local land surface temperature change induced by afforestation based on satellite observations in Guangdong plantation forests in China. Agric Meteorol, 276–277: 107641

Sun G, Zeng X, Liu X (2007). Effects of moderate high-temperature stress on photosynthesis in three saplings of the constructive tree species of subtropical forest. Acta Ecol Sin, 27(4): 1283–1290

Sun Y, Cao F, Wei X, Welham C, Chen L, Pelz D, Yang Q, Liu H (2017). An ecologically based system for sustainable agroforestry in subtropical and tropical forests. Forests, 8(4): 1–18

Sun Y, Wu J, Shao Y, Zhou L, Mai B, Lin Y, Fu S (2011). Responses of soil microbial communities to prescribed burning in two paired vegetation sites in southern China. Ecol Res, 26(3): 669–677

Theil H (1992). A rank-invariant method of linear and polynomial regression analysis. Nederl akad wetensch proc, 12(2): 345–381

Upgupta S, Sharma J, Jayaraman M, Kumar V, Ravindranath N (2015). Climate change impact and vulnerability assessment of forests in the Indian Western Himalayan region: a case study of Himachal Pradesh, India. Clim Risk Manage, 10(2): 63–76

van Leeuwen W, Casady G, Neary D, Bautista S, Alloza J A, Carmel Y, Wittenberg L, Malkinson D, Orr B J (2010). Monitoring post-wildfire vegetation response with remotely sensed time-series data in Spain, USA and Israel. Int J Wildland Fire, 19(1): 75–93

Vermote E, Justice C, Claverie M, Franch B (2016). Preliminary analysis of the performance of the Landsat 8/OLI land surface reflectance product. Remote Sens Environ, 185(2): 46–56

Wang H (2018). Assessing forest disturbance, post-fire forest recovery and its coupling mechanism for climate change. Dissertation for the Master's Degree. Nanjing: Nanjing Forestry University (in Chinese)

Wang W, He H, Thompson F III, Fraser J, Dijak W (2016). Landscape- and regional-scale shifts in forest composition under climate change in the Central Hardwood Region of the United States. Landsc Ecol, 31(1): 149–163

Wu L (2014). Forest disturbance detection by remote sensing: a case

study of Jiangxi Province. Dissertation for the Master's Degree. Nanjing: Nanjing University of Information Science & Technology

Xin Q, Olofsson P, Zhu Z, Tan B, Woodcock C (2013). Toward near real-time monitoring of forest disturbance by fusion of MODIS and Landsat data. Remote Sens Environ, 135: 234–247

Xu Z (1999). A discussion of forestry pollcy in Guangdong Province. Journal of Southwest Forestry College, 02: 105–108

Zhan X, Liang X, Xu G, Zhou L (2013). Influence of plant root morphology and tissue composition on phenanthrene uptake: stepwise multiple linear regression analysis. Environ Pollut, 179: 294–300

Zhao F, Huang C, Zhu Z (2015). Use of vegetation change tracker and support vector machine to map disturbance types in Greater Yellowstone ecosystems in a 1984–2010 landsat time series. IEEE Geosci Remote Sens Lett, 12(8): 1650–1654

Zhao Z, Wang H, Du J, Bai X, Geng S, Wan F (2016). Spatial distribution of forest carbon based on GIS and geostatistical theory in a small Earth-Rocky Mountainous Area of North China. J Biobased Mater Bioenergy, 10(2): 90–99

Zhen Y, Sun P, Liu S (2011). Response of normalized difference vegetation index in main vegetation types to climate change and their variations in different time scales along a North-South Transect of Eastern China. Acta Phytoecol Sin, 35(11): 1117–1126

Zhou B, Gu L, Ding Y, Shao L, Wu Z, Yang X, Li C, Li Z, Wang X, Cao Y, Zeng B, Yu M, Wang M, Wang S, Sun H, Duan A, An Y, Wang X, Kong W (2011). The great 2008 Chinese ice storm: its socio-economic-ecological impact and sustainability lessons learned. Bull Am Meteorol Soc, 92(1): 47–60